PHYSICAL REVIEW C VOLUME 48, NUMBER 3 SEPTEMBER 1993

Alpha scattering and capture reactions in the $A = 7$ system at low energies

P. Mohr, H. Abele, R. Zwiebel, and G. Staudt
Physikalisches Institut der Universität Tübingen, D-7400 Tübingen, Germany

H. Krauss and H. Oberhummer
Institut für Kernphysik, Technische Universität Wien, A-1040 Wien, Austria

A. Denker, J. W. Hammer, and G. Wolf
Institut für Strahlenphysik, Universität Stuttgart, D-7000 Stuttgart, Germany
(Received 13 May 1993)

Differential cross sections for ^{3}He-α scattering were measured in the energy range up to 3 MeV. These data together with other available experimental results for ^{3}He $+\alpha$ and ^{3}H $+\alpha$ scattering were analyzed in the framework of the optical model using double-folded potentials. The optical potentials obtained were used to calculate the astrophysical S factors of the capture reactions ^{3}He$(\alpha,\gamma)^7$Be and ^{3}H$(\alpha,\gamma)^7$Li, and the branching ratios for the transitions into the two final ^{7}Be and ^{7}Li bound states, respectively. For ^{3}He$(\alpha,\gamma)^7$Be excellent agreement between calculated and experimental data is obtained. For ^{3}H$(\alpha,\gamma)^7$Li an $S(0)$ value has been found which is a factor of about 1.5 larger than the adopted value. For both capture reactions a similar branching ratio of $R = \sigma(\gamma_1)/\sigma(\gamma_0) \approx 0.43$ has been obtained.

PACS number(s): 25.55.Ci, 25.70.Jj, 21.60.Gx

I. INTRODUCTION

The reaction ^{3}He$(\alpha,\gamma)^7$Be determines together with other reactions the branching ratio between the *pp*I and (*pp*II + *pp*III) chain in hydrogen burning of main-sequence stars. The magnitude of the cross section of this capture reaction is of special interest for the solar neutrino problem [1]. The mirror reaction ^{3}H$(\alpha,\gamma)^7$Li is the main source for ^{7}Li production in primordial nucleosynthesis [2].

Experimental data for the ^{3}He$(\alpha,\gamma)^7$Be cross section at sub-Coulomb energies have first been obtained by Parker and Kavanagh [3]. Further experiments observing the capture γ rays have been performed by Nagatani, Dwarakanath, and Ashery [4], Kräwinkel *et al.* [5], Osborne *et al.* [6], Alexander *et al.* [7], and Hilgemeier *et al.* [8]. Capture cross sections observing the decay of the ^{7}Be residual nucleus have been measured by Osborne *et al.* [6], Robertson *et al.* [9], Volk *et al.* [10], and Hilgemeier *et al.* [8]. Theoretically, Tombrello and Parker [11] have first succeeded in describing the energy dependence of the astrophysical S factor very well in a direct-capture model. Further calculations in the framework of the potential model have been carried out by Kim, Izumoto, and Nagatani [12] and Buck, Baldock, and Rubio [13]. Analyses using microscopic theories based on the resonating group method have been performed by Walliser, Kanada, and Tang [14], Kajino and Arima [15], Mertelmeier and Hofmann [16], Langanke [17], Kajino [18], and Liu, Kanada, and Tang [19]. The adopted value for the astrophysical S factor chosen by Bahcall [1] to calculate the expected solar neutrino flux is $S(0) = (0.54 \pm 0.03)$ keV b.

In the case of the ^{3}H$(\alpha,\gamma)^7$Li reaction three sets of experimental data at sub-Coulomb energies are published by Griffith *et al.* [20], Schröder *et al.* [21], and Burzynski *et al.* [22]. Several microscopic calculations have been performed in order to analyze this reaction [15–18,23,24]. The presently adopted S-factor value used in standard hot big bang model studies is given by $S(0) = 0.064$ keV b [25].

In this work we analyze the experimental data of both capture reactions, ^{3}He$(\alpha,\gamma)^7$Be and ^{3}H$(\alpha,\gamma)^7$Li, for energies $E_{\rm c.m.} \leq 1.4$ MeV and 0.6 MeV, respectively. The calculations were performed in the framework of the direct-capture model. The most important ingredients in this model are the optical potentials for the bound and scattering states. These potentials are determined using the folding procedure. The strengths of these potentials are adjusted to the experimental scattering data. Therefore, we measured the differential cross sections for ^{3}He-^{4}He elastic scattering in the range $E_{\rm lab}$ (^{3}He) ≤ 3 MeV.

In the next section we describe the direct capture model and the folding procedure for the optical and bound state potentials. In Sec. III we present the ^{3}He-^{4}He and ^{3}H-^{4}He cluster potentials derived from elastic scattering measurements. Finally, in Sec. IV the results for the astrophysical S factors of the capture reactions are given and compared with the experimental data. A summary is given in Sec. V.

II. DIRECT-CAPTURE MODEL AND FOLDING PROCEDURE

Potential models are based on the description of the dynamics of nuclear processes by a Schrödinger equation with local potentials in the entrance and exit channels. Such models are the optical model (OM) for elastic scat-

tering, the distorted-wave Born approximation (DWBA) for transfer and the direct capture model (DC) for direct capture reactions.

The most important ingredients in the potential models are the wave functions for the scattering and bound states in the entrance and exit channels. In calculations performed by our group the potentials are determined by using the folding procedure. In this approach the number of open parameters is reduced considerably compared to more phenomenological potentials (e.g., Saxon–Woods potentials). The nuclear densities are derived from nuclear charge distributions [26] and folded with an energy- and density-dependent nucleon–nucleon (NN) interaction $v_{\rm eff}$ [27–29]:

$$V(R) = \lambda V_{\rm F}(R) = \lambda \int\int \rho_a(\mathbf{r_1})\rho_A(\mathbf{r_2}) \times v_{\rm eff}(E,\rho_a,\rho_A,s)d\mathbf{r_1}d\mathbf{r_2} \quad . \tag{1}$$

The variable s in the NN interaction term is given by

$$s = |\mathbf{R} + \mathbf{r_2} - \mathbf{r_1}| \tag{2}$$

with $\mathbf{R}$ being the separation of the centers of mass of the two colliding nuclei. The normalization factor λ accounts for Pauli repulsion effects and dispersive parts in the potential $V(R)$ which are not included in the folding potential $V_F(R)$. This parameter can be adjusted to elastic scattering data and/or to bound and resonant state energies of nuclear cluster states. At the low energies considered in the nucleosynthesis often the imaginary term in the potential can be neglected. Therefore, in the potential model combined with the folding procedure for the potential the reaction cross sections can be calculated in many cases without any free parameter.

The DC cross section is given by [30]

$$\sigma^{\rm DC} = \int d\Omega \frac{d\sigma^{\rm DC}}{d\Omega} = \int d\Omega\, 2\left(\frac{e^2}{\hbar c}\right)\left(\frac{\mu c^2}{\hbar c}\right)\left(\frac{k_\gamma}{k_a}\right)^3 \frac{1}{2I_A+1}\,\frac{1}{2S_a+1} \times \sum_{M_A M_a M_B \sigma} |\, T_{M_A M_a M_B,\sigma}\,|^2 \quad . \tag{3}$$

The quantities I_A, I_B, and S_a (M_A, M_B, and M_a) are the spins (magnetic quantum numbers) of the target nucleus A, residual nucleus B, and projectile a, respectively. The reduced mass in the entrance channel is given by μ. The polarization σ of the electromagnetic radiation can be ± 1. The wave number in the entrance channel and for the emitted radiation is given by k_a and k_γ, respectively.

The multipole expansion of the transition matrices $T_{M_A M_a M_B,\sigma}$ including electric dipole ($E1$) and quadrupole ($E2$) transitions as well as magnetic dipole ($M1$) transitions is given by

$$T_{M_A M_a M_B,\sigma} = T^{E1}_{M_A M_a M_B,\sigma}\, d^1_{\delta\sigma}(\theta) + T^{E2}_{M_A M_a M_B,\sigma}\, d^2_{\delta\sigma}(\theta) + T^{M1}_{M_A M_a M_B,\sigma}\, d^1_{\delta\sigma}(\theta) \quad . \tag{4}$$

The rotation matrices depend on the angle between $\mathbf{k}_a$ and $\mathbf{k}_\gamma$, which is denoted by θ, where $\delta = M_A + M_a - M_B$.

Defining

$$C(E1) = i\,\mu\left(\frac{Z_a}{m_a} - \frac{Z_A}{m_A}\right) \quad , \tag{5}$$

$$C(E2) = \frac{k_\gamma}{\sqrt{12}}\,\mu^2\left(\frac{Z_a}{m_a^2} + \frac{Z_A}{m_A^2}\right) \quad , \tag{6}$$

we can write for the transition matrices for the electric dipole ($E\mathcal{L} = E1$) or quadrupole ($E\mathcal{L} = E2$) transition

$$T^{E\mathcal{L}}_{M_A M_a M_B,\sigma} = \sum_{l_a j_a} i^{l_a}(l_a\,0\,S_a\,M_a \mid j_a\,M_a)(j_b\,M_B - M_A\,I_A\,M_A \mid I_B\,M_B) \times (\mathcal{L}\,\delta\,j_b\,M_B - M_A \mid j_a\,M_a)\,C(E\mathcal{L})\,\hat{l}_a\,\hat{l}_b\,\hat{j}_b \times (l_b\,0\,\mathcal{L}\,0 \mid l_a\,0)\,\mathcal{W}(\mathcal{L}\,l_b\,j_a\,S_a;\,l_a\,j_b)\,I^{E\mathcal{L}}_{l_b j_b I_B; l_a j_a} \quad . \tag{7}$$

In the above expressions Z_a, Z_A and m_a, m_A are the charge and mass numbers of the projectile a and target nucleus A, respectively. The quantum numbers for the channel spin in the entrance channel and for the transferred angular momentum are denoted by j_a and j_b, respectively.

For magnetic dipole transitions ($M\mathcal{L} = M1$) we obtain

$$T^{M\mathcal{L}}_{M_A M_a M_B,\sigma} = \sum_{l_a j_a} i^{l_a}\,\sigma \Bigg\{ (l_a\,0\,S_a\,M_a \mid j_a\,M_a)(j_b\,M_B - M_A\,I_A\,M_A \mid I_B\,M_B)(1\,\delta\,j_b\,M_B - M_A \mid j_a\,M_a) \times \Bigg[\mu\left(\frac{Z_A}{m_A^2} + \frac{Z_a}{m_a^2}\right)\hat{l}_b\,\hat{j}_b\,\sqrt{l_a(l_a+1)}\,\mathcal{W}(1\,l_a\,j_a\,S_a;\,l_a\,j_b) + 2\mu_a(-1)^{j_b-j_a}\,\hat{S}_a\,\hat{j}_b\,\sqrt{S_a(S_a+1)}\,\mathcal{W}(1\,S_a\,j_a\,l_a;\,S_a\,j_b)\Bigg] - (l_a\,0\,S_a\,M_a \mid j_a\,M_a)(j_a\,M_a\,I_A\,M_B - M_a \mid I_B\,M_B)(I_A\,M_B - M_a\,1\,\delta \mid I_A\,M_A) \times \mu_A\,\delta_{j_a j_b}\sqrt{(I_A+1)/I_A}\Bigg\}\left\{\frac{\hbar c}{2m_{\rm p}c^2}\right\}\delta_{l_a l_b}\,\hat{l}_a\,I^{M1}_{l_b j_b I_B; l_a j_a} \quad , \tag{8}$$

where W is the Racah coefficient, the μ_i are the magnetic moments, and m_p is the mass of the proton.

The overlap integrals in Eqs. (7) and (8) are given as

$$I^{E\mathcal{L}}_{l_bj_bI_B;l_aj_a} = \int dr\, u_{NLJ}(r)\, \mathcal{O}^{E\mathcal{L}}(r)\, \chi_{l_aj_a}(r) \qquad (9)$$

for the electric dipole ($E\mathcal{L} = E1$) or quadrupole ($E\mathcal{L} = E2$) transition, and by

$$I^{M1}_{l_bj_bI_B;l_aj_a} = \int dr\, u_{NLJ}(r)\, \mathcal{O}^{M1}(r)\, \chi_{l_aj_a}(r) \qquad (10)$$

for the magnetic dipole transition ($M\mathcal{L} = M1$).

The radial part of the bound state wave function in the exit channel and the scattering wave function in the entrance channel is given by $u_{NLJ}(r)$ and $\chi_{l_aj_a}(r)$, respectively. The radial parts of the electromagnetic multipole operators are [31]

$$\mathcal{O}^{M1}(r) = \frac{1}{2\rho}\left[\sin\rho + \rho\cos\rho\right] \quad , \qquad (11)$$

$$\mathcal{O}^{E1}(r) = \frac{3}{\rho^3}\left[(\rho^2-2)\sin\rho + 2\rho\cos\rho\right] r \quad , \qquad (12)$$

$$\mathcal{O}^{E2}(r) = \frac{15}{\rho^5}\left[(5\rho^2-12)\sin\rho + (12-\rho^2)\rho\cos\rho\right] r^2 \quad . \qquad (13)$$

In the long wavelength approximation — applicable in our case, since $\rho = k_\gamma r \ll 1$—these quantities reduce to

$$\mathcal{O}^{M1}(r) \simeq 1 \quad , \qquad (14)$$

$$\mathcal{O}^{E1}(r) \simeq r \quad , \qquad (15)$$

$$\mathcal{O}^{E2}(r) \simeq r^2 \quad . \qquad (16)$$

III. ^{3}He - ^{4}He AND ^{3}H - ^{4}He CLUSTER POTENTIALS

At incident energies $E_{\rm lab}(^3{\rm He}) \approx 3 - 10$ MeV differential cross sections for the elastic ^{3}He - ^{4}He scattering are well known [32–36]. In order to obtain cross section data at very low energies we have measured these scattering processes at 20 energies in the range from 1 to 3.3 MeV using the windowless, differential pumped and recirculating gas target system RHINOCEROS installed at the Stuttgart Dynamitron accelerator [37]. In our experiment we used the jet configuration in which a supersonic jet produced by a laval nozzle serves as a nearly pointlike target zone with high density [38]. The small and fixed size of this zone allows a good determination of angular distributions.

The target zone is centered in a 50-cm-diam scattering chamber. The detector system consisted of ten surface-barrier detectors mounted at fixed positions. ^{3}He-beam intensities between 5 and 30 μA were used. In order to normalize the data (assuming that the ^{3}He-^{20}Ne scattering is dominated in this energy range by Rutherford interaction), a small quantity of ^{20}Ne gas was admixed to the ^{4}He gas in the jet.

The experimental differential cross sections for the ^{3}He - ^{4}He scattering are shown together with older data of Barnard, Jones, and Phillips [32] and Chuang [34] in Fig. 1. The results of different phase-shift analyses [33, 35, 36] for projectile energies $E_{\rm lab}(^3{\rm He}) > 3$ MeV are presented in Fig. 2.

We have calculated the differential cross sections and phase shifts in the framework of the OM. For the calculation of the real part of the optical ^{3}He - ^{4}He potential we used the folding procedure as described in Sec. II. The folding potentials [Eq. (1)] were determined using the computer code DFOLD [39]. The imaginary part was neglected because the flux into other channels is very small. Together with the spin-orbit term, the optical potential is given by

$$V(R) = \lambda V_F(R) + \lambda_{\rm s.o.}\frac{1}{R}\frac{dV_F(R)}{dR}\mathbf{L}\cdot\mathbf{s} \qquad (17)$$

with a spin-orbit normalization factor $\lambda_{\rm s.o.}$.

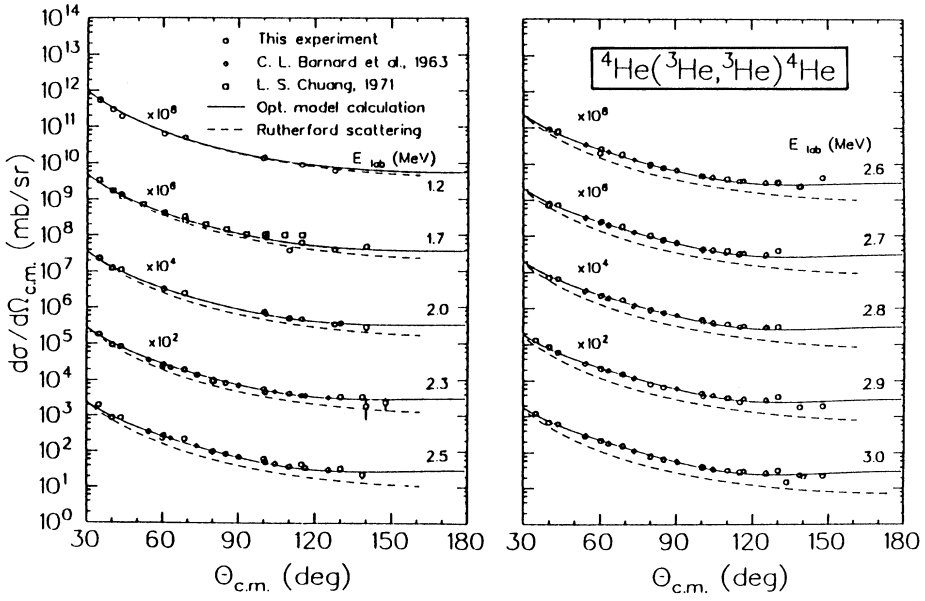

FIG. 1. Experimental differential cross section for the elastic ^{3}He-^{4}He scattering for projectile energies between $E_{\rm lab}(^3{\rm He}) = 1.2$ and 3.0 MeV together with data of Barnard, Jones, and Phillips [32] and Chuang [34]. The solid lines are the result of the present OM calculation, the dashed lines give Rutherford scattering.

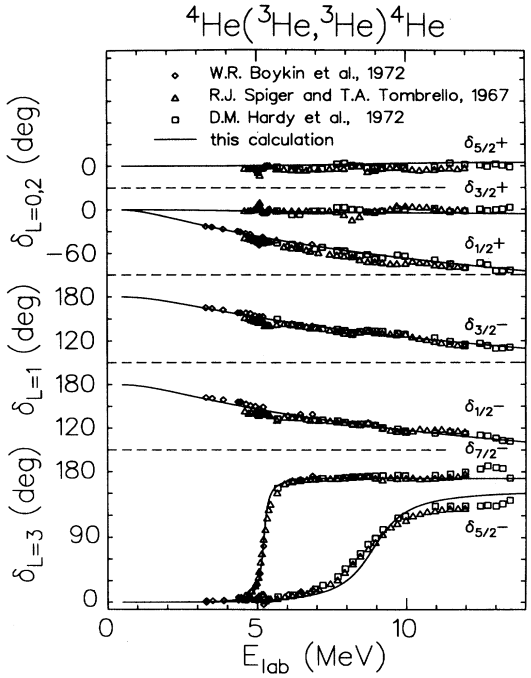

FIG. 2. Phase shifts deduced from experimental ^{3}He-^{4}He scattering data given by Spiger and Tombrello (Δ, [33]), Boykin, Baker, Hardy ($\diamond$, [35]) and Hardy *et al.* ($\square$, [36]). The solid lines are the result of the present OM calculation.

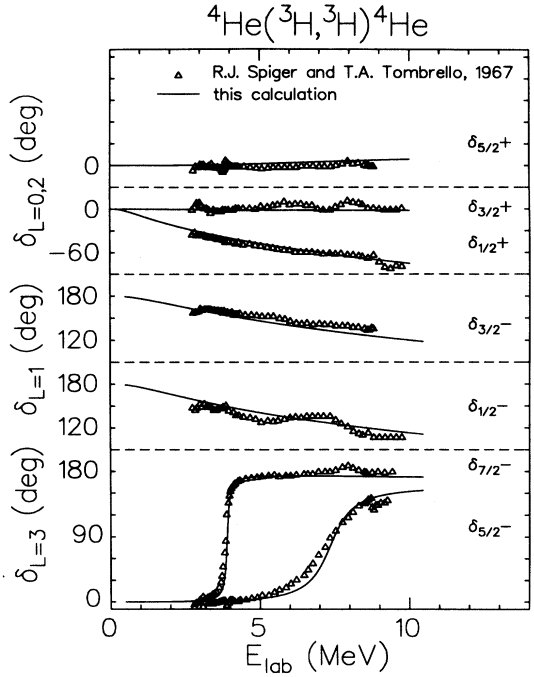

FIG. 3. Phase shifts deduced from experimental ^{3}H-^{4}He scattering data given by Spiger and Tombrello [33]. The solid lines are the result of the present OM calculations.

As result of a fit to the experimental data given in Figs. 1 and 2 we obtain a parity-dependent potential. The normalization factors λ together with the volume integrals per nucleon pair J_R are listed in the upper part of Table I. The spin-orbit normalization factor $\lambda_{s.o.} = -0.162$ fm^2 has been determined from the splitting of the phase shifts for the $L = 3$ doublet. The agreement between the experimental data and the results of the OM calculation is excellent in the whole energy range up to 14 MeV as can be seen in Figs. 1 and 2.

For the ^{3}H - ^{4}He system phase-shift analyses of experimental cross section data have been performed in the energy range $E_{lab}(^3\text{H}) = 3 - 10$ MeV [33]. We have calculated these phase-shifts in the OM. The optical potential is again determined using the folding procedure. The result of our OM fit to the phase–shift data is shown in Fig. 3. The normalization factors λ together with the volume integrals per nucleon pair J_R are presented in the lower part of Table I. For the spin-orbit normalization factor $\lambda_{s.o.}$ now we obtain $\lambda_{s.o.} = -0.136$ fm^2. Again the agreement between the experimental and calculated data is satisfactory (see Fig. 3).

TABLE I. Normalization factors λ and volume integrals per nucleon J_R of the optical potentials.

	Partial wave	λ	J_R (MeV/fm^3)
^{3}He-α	Even (s,d)	1.452	469.0
	Odd (p,f)	1.844	595.6
^{3}H-α	Even (s,d)	1.525	466.8
	Odd (p,f)	1.890	578.5

The volume integrals of the parity-dependent potentials for α scattering on the mirror nuclei ^{3}He and ^{3}H only differ by about 0.5% and 3% for the even and odd partial waves, respectively. The values of the volume integrals for the even partial waves in ^{3}He - α and ^{3}H - α scattering is comparable with the value $J_R = 445.7$ MeV fm^3 obtained in the analysis of α - α scattering using the folding procedure [40]. Furthermore, the values of J_R for ^{3}He - α scattering are compatible with the results of a systematic analysis of ^{3}He scattering on several nuclei [41, 42].

In a next step we used the double-folded potential as a suitable cluster-cluster potential and calculated bound states and single-particle (single-cluster) resonances. The wave function $u_{NLJ}(r)$, which describes the relative motion of the respective ^{3}He - α and ^{3}H - α system is characterized by the node number N and the orbital angular momentum L. The N and L values are related to the corresponding quantum numbers n_i and l_i of the three nucleons forming the ^{3}He and ^{3}H clusters, respectively:

$$Q = 2N + L = \sum_{i=1}^{3} 2n_i + l_i = \sum_{i=1}^{3} q_i = 3 \ . \qquad (18)$$

Thus for both systems ^{7}Be = ^{3}He $\otimes$ α and ^{7}Li = ^{3}H $\otimes$ α one expects two cluster states with $L = 1$ $(N = 1)$ and $L = 3$ $(N = 0)$. Both states split into doublets with

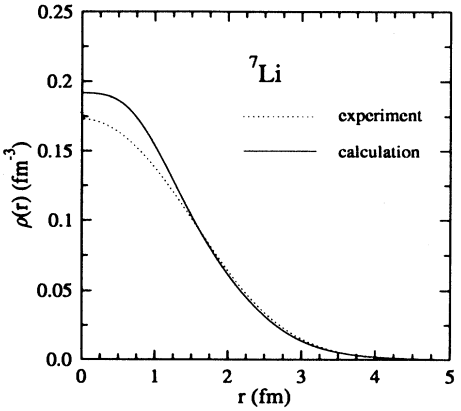

FIG. 4. Comparison of the experimental charge distribution of ^{7}Li [26] (dashed line) with the distribution calculated in the potential model (solid line).

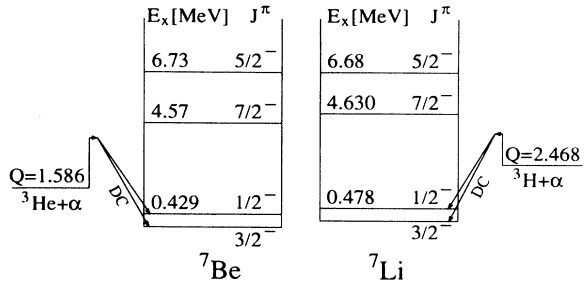

FIG. 5. Schematic presentation of the level scheme for the reactions ^{3}He$(\alpha,\gamma)^7$Be and ^{3}H$(\alpha,\gamma)^7$Li.

$J = L \pm 1/2$ because of the spin-orbit potential resulting from the motion of the $A = 3$ particle with spin 1/2 in the field of the α particle.

In the calculations of the cluster states the centroid energies of both the bound ($L = 1 : J^\pi = 3/2^-, 1/2^-$) and quasibound ($L = 3 : J^\pi = 7/2^-, 5/2^-$) states for ^{7}Be and ^{7}Li (see Fig. 5) are reproduced by the central parts of the ^{3}He - α and ^{3}H - α odd potentials, respectively. The splitting of the energies of the quasibound state doublets ($L = 3$) in ^{7}Be and ^{7}Li is reproduced by the spin-orbit potential as determined by the OM calculation. However, for the bound-state doublets ($L = 1$) in ^{7}Be and ^{7}Li smaller spin-orbit potentials are necessary. For the energy splitting of the bound-state doublets a spin-orbit normalization factor $\lambda_{\text{s.o.}} = -0.07$ fm^2 has to be used for both nuclei ^{7}Be and ^{7}Li.

As a further test of our folding potential we calculated the charge distribution of the ^{7}Li nucleus (in its ground state) by folding the experimental charge distribution of ^{3}H and ^{4}He, which we have already used in our double-folding procedure, with the radial wave function $u_{N=1,L=1,J=3/2}$ and by assuming a spherical shape for the folded distribution. The result of this calculation is shown in Fig. 4 together with the experimental charge distribution, as measured by electron scattering on ^{7}Li. It can be seen that the calculation overestimates the experimental density in the nuclear interior, whereas in the surface region, near $r = 2.5$ fm, the experimental values are slightly underestimated. But the rms radii of both distributions are almost identical: $\langle r^2\rangle^{1/2} \approx 2.40$ fm.

IV. CAPTURE REACTIONS

In Fig. 5 a schematic presentation of the direct capture processes ^{3}He$(\alpha,\gamma)^7$Be and ^{3}H$(\alpha,\gamma)^7$Li is given. In the low-energy range capture transitions can only occur into the ground and first excited states of ^{7}Be and ^{7}Li, respectively.

The theoretical cross section σ^{th} is obtained from the DC cross section σ^{DC}, given in Eq. (3), as sum over both final states $i = 1, 2$ by

$$\sigma^{\text{th}} = \sum_i C_i^2 S_i \sigma_i^{\text{DC}} \quad . \tag{19}$$

The computation of the cross section σ^{th} was performed using the computer code TEDCA [43]. As input three data sets are necessary: (i) isospin Clebsch-Gordan coefficients, (ii) spectroscopic factors S_i, which specify the cluster probability of the final states ^{7}Be = ^{3}He $\otimes$ α and ^{7}Li = ^{3}H $\otimes$ α, respectively, and (iii) optical potentials for the calculation of the wave functions in the entrance and exit channel. In our case the Clebsch-Gordan coefficients are $C_i = 1$. The spectroscopic factors S_i have been taken from the work of Kurath and Millener [44]. The numerical values are given as $S_1 = 1.174$ and $S_2 = 1.175$. In order to calculate the bound state wave function in the exit channel and the scattering wave function in the entrance channel [Eqs. (9) and (10)], the folded potentials are used, which have already been determined in Secs. II and III. That means that all the necessary information for the calculation of the DC reaction is known and no parameter has to be adjusted to the experimental capture reaction data.

In Fig. 6 the experimental values of the astrophysical S factor for the reactions ^{3}He$(\alpha,\gamma)^7$Be [5, 6, 8] and ^{3}H$(\alpha,\gamma)^7$Li [20, 21] are shown together with the results of DC calculations using parity-dependent folding potentials. The experimental data of Kräwinkel *et al.* [5] are renormalized by a factor of 1.4 as suggested by Hilgemeier *et al.* [8].

For the ^{3}He$(\alpha,\gamma)^7$Be reaction the agreement between the experimental and calculated data is excellent. A linear extrapolation for $E \to 0$ gives $S(0) = 0.516$ keV b and $\dot{S}(0) = -3.67 \times 10^{-4}$ b (E in keV). The values of $S(0)$ agree excellently with the experimentally determined $S(0)$ factor, for which [8] gives a weighted average of $S(0) = (0.51 \pm 0.02)$ keV b, and with the adopted value [1] of $S(0) = (0.54 \pm 0.03)$ keV b. The calculated branching ratio R for the transitions to the first excited state and the ground state has the value $R = 0.43$. This value was found to be nearly energy independent in the energy range 0 – 1.4 MeV and agrees well with both the experimental data [5, 6, 8] and the results of microscopic calculations [24].

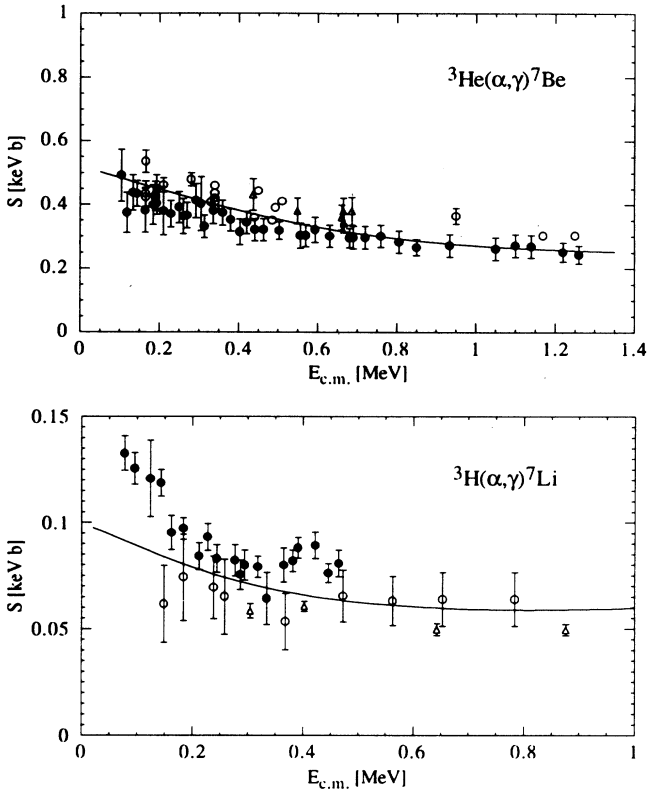

FIG. 6. Calculated astrophysical S factor using the potential model compared with the experimental data for $^3\mathrm{He}(\alpha,\gamma)^7\mathrm{Be}$ (upper part: closed circles [5], open circles [6], triangles [8]), and $^3\mathrm{H}(\alpha,\gamma)^7\mathrm{Li}$ (lower part: open circles [20], closed circles [21], triangles [22]).

The two presently available measurements of the low-energy $^3\mathrm{H}(\alpha,\gamma)^7\mathrm{Li}$ reaction differ from each other by roughly 30% in total magnitude as well as in their determination of the branching ratios for the transitions into the two final bound states. The calculation within the potential model gives results for the absolute magnitude of the S factor which favor rather the older experimental data of Griffith *et al.* [20]. The calculated branching ratio is again nearly energy independent and has likewise a value of $R = 0.43$. This branching ratio, however, is noticeably larger than the experimentally observed value $R = 0.32 \pm 0.01$ [21]. Our value agrees with the data of [20], which give an energy-independent average of $R = 0.43$ [24]. The above considerations are comparable with the results of microscopic resonating group method (RGM) calculations [24]. A linear extrapolation for $E \to 0$ gives $S(0) = 0.100$ keV b and $\dot{S}(0) = -1.02 \times 10^{-4}$ b (E in keV). The values of $S(0)$ are nearly twice as large as the adopted value of 0.064 keV b [25], obtained from an energy-independent extrapolation, and somewhat smaller than the extrapolated value 0.14 keV b extracted from the data of Schröder *et al.* [21]. However, it is in excellent agreement with the results of different RGM calculations [16–18, 23, 24] giving a value of $S(0) \approx 0.1$ keV b.

In Fig. 7 the multipole contributions for both capture reactions are shown. The main contribution is the $E1$ transition. Because of the missing centrifugal barrier, the DC transitions from the s wave in the entrance channel to the final $L = 1$ states are dominating. For the $^3\mathrm{H}(\alpha,\gamma)^7\mathrm{Li}$ reaction the contributions of the higher partial waves for the total S factor can even be neglected. As can be seen on the right-hand side of Fig. 7 the curve of the total S factor is almost identical to the s-wave contribution. The Coulomb barrier is lower for $^3\mathrm{H}(\alpha,\gamma)^7\mathrm{Li}$ than for the mirror reaction. Therefore, the influence of the centrifugal barrier is more pronounced.

As already discussed in Sec. III, a parity-dependent optical potential is necessary to describe the experimental scattering data. We calculated the astrophysical S factor with a parity-independent potential using the λ parameter for the dominating even partial waves given in Table I. As shown in Fig. 8, it is impossible to reproduce the experimental data with such a parity-independent potential. The enhancement for energies $E \geq 0.7$ MeV is due to the $M1$ contribution of the p wave.

We also tested the sensitivity of the astrophysical S factor by changing the strength of the optical potentials

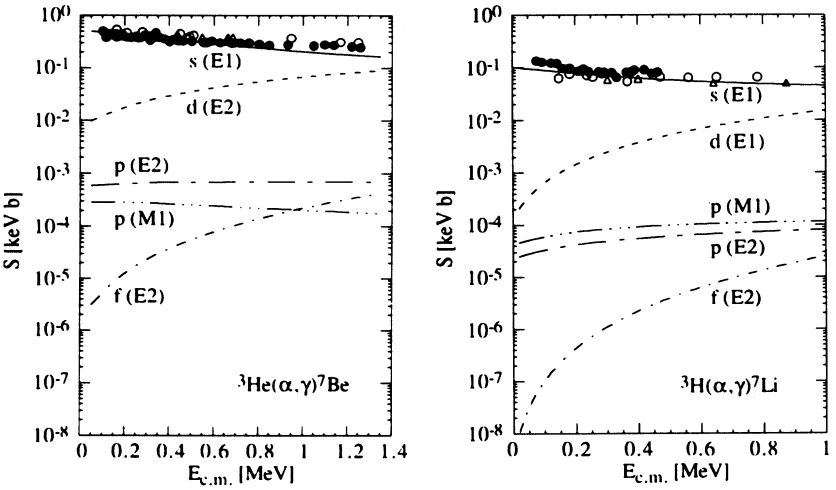

FIG. 7. Multipole contributions to the astrophysical S factors for the reaction $^3\mathrm{He}(\alpha,\gamma)^7\mathrm{Be}$ (left-hand side) and $^3\mathrm{H}(\alpha,\gamma)^7\mathrm{Li}$ (right-hand side). The experimental data are the same as in Fig. 6.

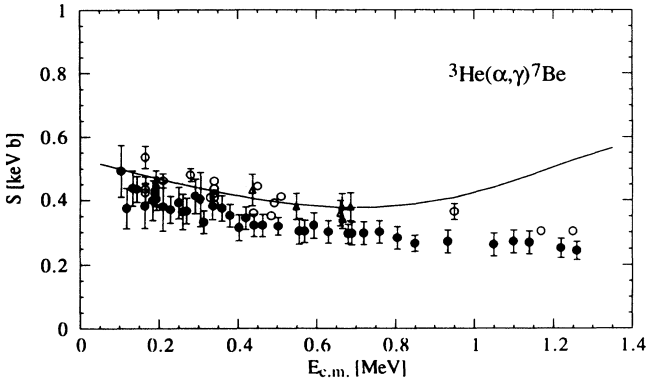

FIG. 8. S factor for ^{3}He$(\alpha,\gamma)^7$Be calculated with a parity-independent potential in the entrance channel. The experimental data are the same as in Fig. 6.

in the entrance channel. A variation of the potential depth of $\pm 1\%$ leads to an energy-independent change of the S factor of $\pm 2\%$. The S factor increases with growing potential depth. The reason for this behavior is that with growing nuclear potential depth the Coulomb barrier becomes smaller and therefore the penetration probability is enhanced.

V. SUMMARY

Differential cross sections for the elastic scattering of ^{3}He particles on ^{4}He and phase shifts of both ^{3}He - ^{4}He and ^{3}H - ^{4}He scattering have been analyzed up to energies of about 10 MeV in the framework of the optical model. The potential was deduced by a double-folding procedure using a density-dependent effective nucleon-nucleon interaction. The experimental data are described satisfactorily by this optical-model calculation.

Using the double-folded ^{3}He-α and ^{3}H-α potentials as cluster-cluster potentials, we calculate the bound and quasibound doublet states in ^{7}Be and ^{7}Li, respectively. The excitation energies of these states as well as the charge distribution of ^{7}Li are well reproduced in this potential model.

The optical potentials obtained from the fit to the elastic scattering data have been used to calculate the astrophysical S factors of ^{3}He$(\alpha,\gamma)^7$Be and ^{3}H$(\alpha,\gamma)^7$Li within the direct capture model. Using this method no parameter has to be adjusted to the experimental reaction data.

In the case of the reaction ^{3}He$(\alpha,\gamma)^7$Be we obtain $S(0) = 0.516$ keV b. This value is in excellent agreement with both the average of the experimental data [8] and the adopted value [1]. The branching ratio for the transitions to the first excited state and the ground-state results in $R = 0.43$, likewise in very good agreement with the known experimental and theoretical data.

For the reaction ^{3}H$(\alpha,\gamma)^7$Li the three presently available measurements differ from each other by roughly 30% in total magnitude as well as in their determination of the branching ratio for the transitions into the two final ^{7}Li bound states. In agreement with calculations, which have been done in the framework of the resonating group method or on the basis of a microscopic potential model, our calculations predict the S factor to increase with decreasing energy resulting in $S(0) = 0.10$ keV b. This value is a factor of about 1.5 larger than the adopted value [25]. For the branching ratio we obtain $R = 0.43$. This value is in good agreement with some theoretical results, but is not compatible with the recently measured value of $R = 0.32 \pm 0.01$ [21].

ACKNOWLEDGMENTS

We would like to thank the Deutsche Forschungsgemeinschaft (DFG Project Sta/2-1), the Österreichische Nationalbank (Project 3924), and the Fonds zur Förderung der wissenschaftlichen Forschung in Österreich (Project P 8806–PNY).

[1] J.N. Bahcall, *Neutrino Astrophysics* (Cambridge University Press, Cambridge, 1989).
[2] G. Steigman, in *Nucleosynthesis:Challenges and New Developments*, edited by W.D. Arnett and J.W. Truran (Chicago, Chicago, 1985), p. 48.
[3] P.D. Parker and R.W. Kavanagh, Phys. Rev. **131**, 2578 (1963).
[4] K. Nagatani, M.R. Dwarakanath, and D. Ashery, Nucl. Phys. **A128**, 325 (1969).
[5] H. Kräwinkel, H.W. Becker, L. Buchmann, J. Görres, K.U. Kettner, W.E. Kieser, R. Santo, P. Schmalbrock, H.P. Trautvetter, A. Vlieks, C. Rolfs, J.W. Hammer, R.E. Azuma, and W.S. Rodney, Z. Phys. A **304**, 307 (1982).
[6] J.L. Osborne, C.A. Barnes, R.W. Kavanagh, R.M. Kremer, G.J. Mathews, J.L. Zyskind, P.D. Parker, and A.J. Howard, Phys. Rev. Lett. **48**, 1664 (1982); Nucl. Phys. **A419**, 115 (1984).
[7] T.K. Alexander, G.C. Ball, W.N. Lennard, H.Geissel, and H.-B. Mak, Nucl. Phys. **A427**, 526 (1984).
[8] M. Hilgemeier, H.W. Becker, C. Rolfs, H.P. Trautvetter, and J.W. Hammer, Z. Phys. A **329**, 243 (1988).
[9] H.G.H. Robertson, P. Dyer, T.J. Bowles, R.E. Brown, N. Jarmie, C.J. Maggiore, and S.M. Austin, Phys. Rev. C **27**, 11 (1983).
[10] H. Volk, H. Kräwinkel, R. Santo, and L. Wallek, Z. Phys. A **310**, 91 (1983).
[11] T.A. Tombrello and P.D. Parker, Phys. Rev. **131**, 2582 (1963).
[12] B.T. Kim, T. Izumoto, and K. Nagatani, Phys. Rev. C **23**, 33 (1981).
[13] B. Buck, R.A. Baldock, and J.A. Rubio, J. Phys. G **11**, L11 (1985).
[14] H. Walliser, H. Kanada, and Y.C. Tang, Nucl. Phys. **A419**, 133 (1984).
[15] T. Kajino and A. Arima, Phys. Rev. Lett. **52**, 739 (1984).
[16] T. Mertelmeier and H.M. Hofmann, Nucl. Phys. **A459**, 387 (1986).

[17] K. Langanke, Nucl. Phys. **A457**, 351 (1986).
[18] T. Kajino, Nucl. Phys. **A460**, 559 (1986).
[19] Q.K.K. Liu, H. Kanada, and Y.F. Tang, Phys. Rev. **33**, 1561 (1986).
[20] G.M. Griffith, R.A. Morrow, P.J. Riley, and J.B. Warren, Can. J. Phys. **39**, 1397 (1961).
[21] U. Schröder, A. Redder, C. Rolfs, R.E. Azuma, L. Buchmann, C. Campbell, J.D. King, and T.R. Donoghue, Phys. Lett. B **192**, 55 (1987).
[22] S. Burzynski, K. Czerski, A. Marcinkowski, and P. Zupranski, Nucl. Phys. **A473**, 179 (1987).
[23] T. Kajino, J. Phys. Soc. Jpn. **54** (Suppl), 321 (1985).
[24] T. Altmeyer, E. Kolbe, T. Warmann, K. Langanke, and H.J. Assenbaum, Z. Phys. A **330**, 277 (1988).
[25] W.A. Fowler, G.R. Caughlan, and B.A. Zimmermann, Ann. Rev. Astron. Astrophys. **5**, 525 (1967); **13**, 69 (1975).
[26] H. de Vries, C.W. Jager, and C. de Vries, At. Data Nucl. Data Tables **36**, 495 (1987).
[27] A.M. Kobos, B.A. Brown, R. Lindsay, and R. Satchler, Nucl. Phys. **A425**, 205 (1984).
[28] H. Oberhummer and G. Staudt, in *Nuclei in the Cosmos*, edited by H. Oberhummer (Springer, Heidelberg, 1991), p. 29.
[29] H. Abele and G. Staudt, Phys. Rev. C **47**, 742 (1993).
[30] K.H. Kim, M.H. Park, and B.T. Kim, Phys. Rev. C **35**, 363 (1987).
[31] B.G. Bailey, G.M. Griffiths, and T.W. Donnely, Nucl. Phys. **A94**, 502 (1967).
[32] A.C.L. Barnard, C.M. Jones, and G.C. Phillips, Nucl. Phys. **50**, 629 (1964).
[33] R.J. Spiger and T.A. Tombrello, Phys. Rev. **63**, 964 (1967).
[34] L.S. Chuang, Nucl. Phys. **A174**, 399 (1971).
[35] W.R. Boykin, S.D. Baker, and D.M. Hardy, Nucl. Phys. **A195**, 241 (1972).
[36] D.M. Hardy, R.J. Spiger, S.D. Baker, Y.S. Chen, and T.A. Tombrello, Nucl. Phys. **A195**, 250 (1972).
[37] J.W. Hammer, W. Biermayer, T. Griegel, H. Knee, and K. Petkau, Nucl. Instrum. Methods (to be published).
[38] H. Knee, diploma thesis, University of Stuttgart, 1987.
[39] H. Abele, computer code DFOLD, University of Tübingen (unpublished).
[40] H. Abele, Ph.D. thesis, University of Tübingen, 1992.
[41] R. Görgen, F. Hinterberger, R. Jahn, P. von Rossen, and B. Schüller, Nucl. Phys. **A320**, 296 (1979).
[42] H.-J. Trost, A. Schwarz, U. Feindt, F.H. Heimlich, S. Heinzel, J. Hintze, F. Körber, R. Lekebusch, P. Lezoch, G. Möck, W. Paul, E. Roick, M. Wolff, J. Worzeck, and U. Strohbusch, Nucl. Phys. **A337**, 377 (1980).
[43] H. Krauss, computer code TEDCA, TU Wien (unpublished).
[44] D. Kurath and D.J. Millener, Nucl. Phys. **A238**, 269 (1975).